Journal of Dental Sciences

Volume 21 | Issue 2 Article 64

2026

A preclinical overall evaluation of a novel biomimetic collagen membrane for guided tissue regeneration

Kuo-Yi Lin

Yi-Ling Tsai

Che-Yung Kuan

Ying-Chih Lin

Chen-Ying Wang

Journal of Dental Sciences 21 (2026) 1223–1237

Available online at https://jds.ads.org.tw/journal/

Digital Commons

journal homepage: https://jds.ads.org.tw/journal/

Original Article

A preclinical overall evaluation of a novel biomimetic collagen membrane for guided tissue regeneration

Kuo-Yi Lin [a†], Yi-Ling Tsai [a†], Che-Yung Kuan [b,c], Ying-Chih Lin [d], Wen-Yu Su [e], Hao-Hueng Chang [f], Chen-Ying Wang [a,f*]

[a] *Department of Dentistry, National Taiwan University Hospital, Taipei, Taiwan*
[b] *Institute of Biomedical Engineering, College of Medicine and College of Engineering, National Taiwan University, Taipei, Taiwan*
[c] *Institute of Biomedical Engineering and Nanomedicine, National Health Research Institutes, Miaoli, Taiwan*
[d] *Horien Biochemical Technology, Taichung, Taiwan*
[e] *Department of Bioinformatics and Medical Engineering, Asia University, Taichung, Taiwan*
[f] *School of Dentistry, National Taiwan University, Taipei, Taiwan*

Received 24 January 2026; Final revision received 25 January 2026
Available online 1 April 2026

KEYWORDS
Collagen membrane;
Decellularized technique;
Guided tissue regeneration;
Intrabony defect;
Periodontal tissue regeneration

Abstract *Background/purpose:* Guided tissue regeneration (GTR) relies on barrier membranes to facilitate periodontal tissue regeneration. Conventional collagen membranes may require chemical crosslinking, which can compromise biological activity. This study evaluated a novel decellularized small intestinal submucosa (dSIS) membrane prepared using an eco-friendly alkyl polyglycoside (APG) technique and compared its biological and regenerative performance with that of a commercial collagen membrane.

Materials and methods: APG-treated dSIS membranes were characterized and compared with a commercially available collagen membrane (BioGide®; Geistlich Pharma AG, Wolhusen, Switzerland). Amino acid composition, glycosaminoglycan (GAG) content, and growth factor content were analyzed. In vitro osteoblast adhesion and proliferation were assessed using a human fetal osteoblast cell line. Regenerative efficacy was evaluated in a canine one-wall intrabony defect model using histometric analysis, micro-computed tomography, and fluorochrome labeling.

Results: The dSIS membrane preserved the native collagen structure and retained higher levels of GAG and basic fibroblast growth factor than the commercial collagen membrane. Both membranes supported osteoblast adhesion and proliferation without cytotoxic effects. All defects

* Corresponding author. School of Dentistry, National Taiwan University, No. 1, Chang-de Street, Taipei 10048, Taiwan.
E-mail address: jywang8919@ntu.edu.tw (C.-Y. Wang).
† These authors contributed equally to this work.

https://doi.org/10.1016/j.jds.2026.01.023

healed uneventfully in vivo. Although no statistically significant differences were observed among groups due to the limited sample size, membrane-treated groups tended to exhibit greater new bone formation than the negative control group. Earlier bone remodeling was observed in the dSIS group.
Conclusion: We conclude that APG-treated dSIS demonstrates favorable biocompatibility and regenerative potential comparable to that of a conventional collagen membrane. Retention of native biomolecules may enhance the early bone healing, suggesting that the APG-treated dSIS is a promising alternative for periodontal tissue regeneration.

Introduction

Periodontitis is a type of periodontal disease caused by the interaction of bacterial biofilm and the host immune response, which usually leads to the breakdown of the periodontal apparatus. Regenerating the lost periodontal supporting tissue has been the primary goal of many researchers for several years.

The guided tissue regeneration (GTR) surgery has been confirmed useful in periodontal intrabony defects, including gains in clinical attachment level, new bone formation, and periodontal pocket reduction. The GTR involves a dentist performing flap surgery and placing a barrier membrane. The environment created allows cells to selectively repopulate a debrided root surface and form a new periodontal attachment.

The first concept of the GTR was published by Melcher.[1] The study discussed the idea of a type-specific cell repopulation theory of healing. The hypothesis suggests that a selected cell population within a barrier membrane in the periodontium can produce more bone if unwanted cells are excluded. Therefore, based on this theory, a dental membrane used as a barrier plays an important role in the GTR surgery. Scantlebury,[2] Gottlow,[3] and Hardwick et al.[4] proposed design criteria for the GTR membranes. The criteria include biocompatibility, cell exclusion, space maintenance, tissue integration, ease of use, and biological activity. However, these characteristics are sometimes in conflict with the material's design concept. For example, if a chemical crosslinker is used in a resorbable biomaterial, mechanical strength would be enhanced and the resorption time of the dental membrane would be prolonged. This is a merit for space maintenance. However, its bioactivity and biocompatibility may be compromised.[5–7] How to design a suitable membrane for clinical use has become an intriguing problem, and all considerations from the different aspects have to be taken into account.

In clinics, the first prototype of a dental membrane was a cellulose acetate laboratory filter.[8,9] Non-absorbable biomaterials, such as dense or expanded polytetrafluoroethylene (PTFE), have been used for the GTR in the past 30 years.[10,11]

The membranes made from PTFE can maintain their integrity in situ for as long as the operator expects, whereas these membranes require additional surgery to remove. Inconvenience, time, cost, and possible morbidity associated with the surgical procedures would not be in the patient's best interest. Therefore, the absorbable barriers, such as collagen membranes, appeared on the market. Using an absorbable membrane reduces patient discomfort, chair-side time, and costs. However, the advantage of an absorbable membrane is also its disadvantage. The biodegradable membranes, which degrade over time, offer only limited control over the resorption time of the application. As mentioned above, these membranes, such as collagen-based scaffolds, require additional chemical crosslinking to extend their in vivo absorption time, which inevitably creates an undesired cell-adhesive environment and, in turn, a cytotoxic problem.[7,12] Therefore, a non-crosslinked collagen-based membrane, such as the BioGide® (Geistlich Pharma AG, Wolhusen, Switzerland), is generally used as a standard membrane for preclinical comparison.

Recently, a decellularization technique for preparing dental membranes has been developed.[13] Another study showed that the decellularized small intestinal submucosa and polycaprolactone (dSIS-PCL) composite membrane has immense potential as a candidate material for bladder tissue engineering.[14] In the decellularization process, chemical detergents are commonly used to remove cellular components. In current decellularization methodologies, sodium dodecyl sulfate (SDS) is the most widely used detergent for decellularizing small intestinal submucosa. At a low concentration (0.1 %), SDS decellularization is effective while preserving overall tissue dimensions.[15]

The SDS treatment is often combined with a degreasing or disinfecting agent such as N-hexane, peracetic acid (PAA), and Triton X-100. However, whether used independently or in combination, these surfactants and solvents all have drawbacks. The disadvantages of these characteristics have been reported, with unwanted effects that limit clinical application, including possible retention of surfactant in the extracellular matrix (ECM), ECM damage,[16] antigen residues,[17] growth factors,[18] and glycosaminoglycan (GAG) loss.[19,20]

Given the problems listed above, finding an alternative decellularization reagent is urgent. Alkyl polyglycoside (APG), a biodegradable and eco-friendly sugar-based surfactant, has been used in personal care and agricultural applications for years.[21,22] Numerous toxicological tests, including tissue irritation and gene mutation responses, have been conducted, and its toxicological profile has been

outlined.[23,24] A high safety factor (greater than 1000) also indicates that it's relatively safe to use and handle, even in accidental swallowing situations.[25] Therefore, we developed a novel method to decellularize small intestinal submucosa (dSIS) with APG without any further chemical crosslinking treatment.

Given the possible structural and compositional similarity between the acellular matrix and the collagen matrix, we would like to examine the differences between the APG-treated acellular matrix and the traditional collagen matrix in vivo and in vitro. Accordingly, the study preliminarily evaluated the overall performance of the decellularized membrane compared with the commercial collagen membrane (Fig. 1).

Materials and methods

Sample preparation

Preparation of decellularized scaffolds: decellularized small intestinal submucosa (dSIS)

Intestines were collected directly from L-Y-D hogs. All hogs were seven months old, and the average weight of the hogs was 125 kg. All tissues were collected in a licensed slaughterhouse. Collection procedures complied with HACCP and ISO 22442. After harvesting, the intestines were reversed inside out, soaked in 1.5 % alkyl polyglycoside (BASF, Ludwigshafen, Germany), approximately equal to the weight of the harvested tissue, and transferred to the GMP plant. Within 4 h, the intestines were washed with distilled water, at least ten times the tissue weight. The serosa and muscularis mucosae were mechanically delaminated from the intestines and longitudinally cut to form flat sheets, exposing the mucosa. The mucosa layers were then scraped off with a stainless steel scraper. After scraping off the mucosa, the submucosa layers were gently rinsed with the distilled water and soaked in 1.5 % APG overnight. We washed the separated submucosa layers with the trypsin–EDTA (Merck, Darmstadt, Germany) and the distilled water for another 24 h. Then, the submucosa layers were split longitudinally, divided into 30 cm sections, multi-laminated, and treated in sequence with lyophilization (FD), dehydrothermal treatment (DHT),[26] and sterilization. The sterilization method was γ-radiation with a radiation dose of 25 kGy.

Resorbable barrier membrane: BioGide®

Commercial collagen membrane BioGide® was produced from Geistlich Pharma AG (Wolhusen, Switzerland). The dental membranes consist of type I and type III collagen from porcine origin. The processing steps may include purification with strong organic solvents (NaOH/n-hexane/acetone) to remove grease and lipoproteins.[27,28] The processed membrane, with a bilayer microstructure, is said to prevent soft-tissue ingrowth into the augmented site and allow degradation residues to support further regeneration.[29,30]

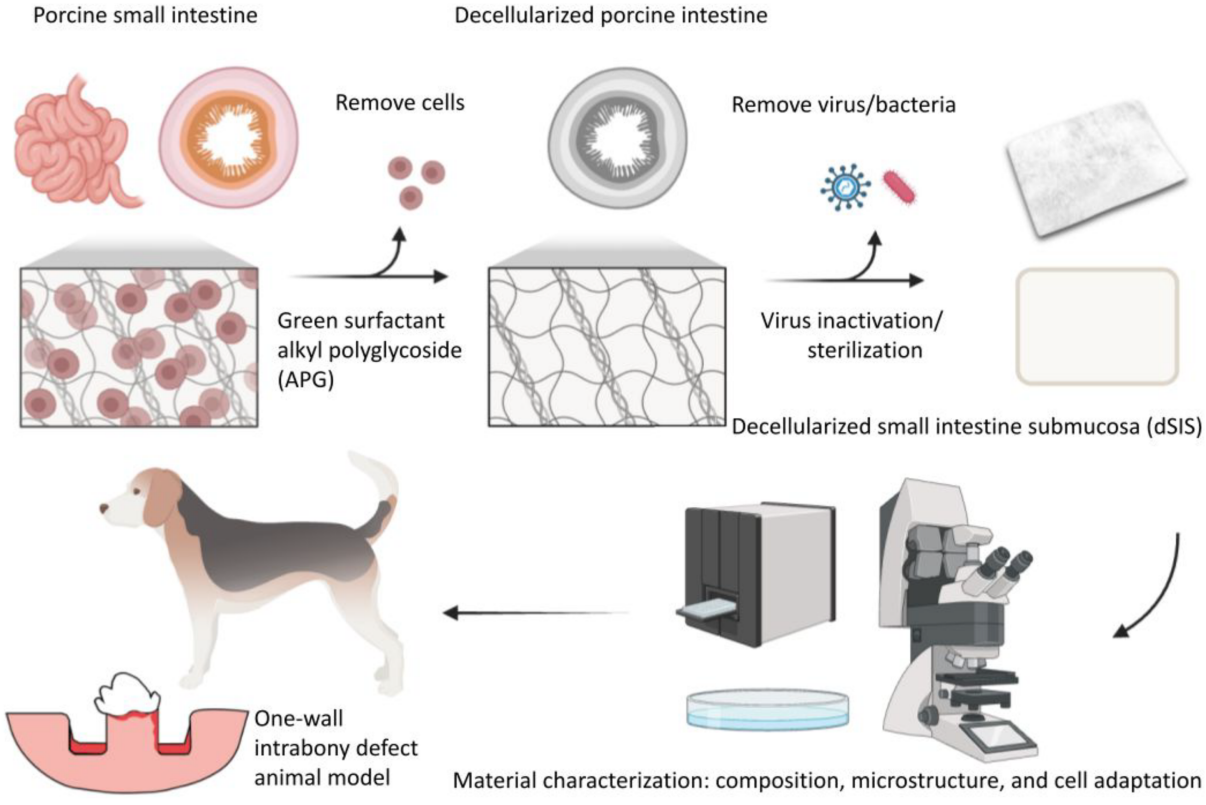

Figure 1 Experimental procedure flowchart. Created with Biorender.com.

Bone substitution material: BioOss®
Bone substitute material BioOss® was also produced from Geistlich Pharma AG (Wolhusen, Switzerland). The material is derived from natural bovine bone. The process includes deorganification with strong alkalis and organic solvents, heating to about 350–400 °C to prepare different types of bone mineral pieces, and milling into small particles.[31] The process allegedly renders the particles non-immunogenic and protein-free. The particle sizes used in the study ranged from 250 μm to 1000 μm.

Characterization of membranes

Amino acid analysis of the decellularized small intestinal submucosa (dSIS) and BioGide®
The sample preparation and the method of amino acid analysis followed the standard methods for amino acid analysis of food.[32] The hydrolyzed samples of the dSIS and BioGide® were analyzed using an amino acid analyzer LA8080 (Hitachi, Tokyo, Japan).

Glycosaminoglycan (GAG) content of the decellularized small intestinal submucosa (dSIS) and BioGide®
The sample preparation and the GAG method followed standard United States Pharmacopeia methods. 25 mg of the dSIS and BioGide® were cut into small pieces (roughly 2 mm × 2 mm). Transfer the sample to a 1.5-ml micro-centrifuge tube, add 180 μL of sterile PBS and 20 μL of proteinase K solution, mix, and incubate at 56 °C for 15 min. Cool the sample to room temperature. Dilute with water to obtain a sample concentration of 12.5 mg per mL. Add 2.5 ml of 1,9-dimethylmethylene blue solution. Mix on a vortex mixer for 1 s, and then immediately read the absorbance at 525 nm using an ELISA reader (BMG LABTECH, Ortenberg, Germany).[33]

Basic fibroblast growth factor/vascular endothelial growth factor (bFGF/VEGF) content of the decellularized small intestinal submucosa (dSIS) and BioGide®
The sample preparation and the method for the bFGF/VEGF followed the standard methods of the United States Pharmacopeia. A 1 cm^2 sample of the dSIS and BioGide® in 400 μl of sterile PBS was pulverized for 90 s using a tissue homogenizer (PRO Scientific, Oxford, CT, USA), intermittently checking to ensure the tissue remained immersed in the sterile PBS and was homogenized. The samples were centrifuged at 12,000 g for 5 min at 4 °C. The supernatant was collected for assays. The bFGF/VEGF concentration was determined using an antibody against human growth factor by a sandwich enzyme-linked immunosorbent assay (ELISA) kit (RayBiotech, Peachtree Corners, GA, USA). The optical density was measured using an ELISA reader (BMG LABTECH, Ortenberg, Germany) at a wavelength of 450 nm.[34]

Microstructure of the decellularized small intestinal submucosa (dSIS) and BioGide®
The inner and outer microstructures of the dSIS and the commercial product were examined by a scanning electron microscope (SEM), Hitachi TM1000 (Hitachi, Tokyo, Japan). All surfaces were sputtered with a gold-palladium alloy before imaging. The operating current was set at 30 mA and discharged for 30 s.

Cell culture study

Decellularized small intestinal submucosa (dSIS) and BioGide® cultured with osteoblast cells (hFOB)
Cut the dSIS and BioGide® membranes into 1 cm diameter circles. Place each sample in a 24-well culture plate (TPP, Trasadingen, Switzerland). Osteoblast cells (hFOB 1.19) were seeded on the testing material on the top of the dSIS and BioGide® at a density of 20×10^4 cells/well. One mL of medium containing DMEM/F12 (D8900, Sigma–Aldrich, St. Louis, MO, USA) + 0.3 mg/ml G418 (10131027, Gibco, Waltham, MA, USA) + 10 % FBS (SH30071, HyClone, Logan, UT, USA) + 1 % antibiotic-antimycotic (15240062, Gibco, Waltham, MA, USA) was added per well. The dSIS and BioGide® membranes were left in the wells for 10 min to fully absorb the medium. The medium was changed every three days.

Scanning electron microscope (SEM) and hematoxylin and eosin stain (H&E) section of the decellularized small intestinal submucosa (dSIS) and BioGide® cultured with osteoblast cells (hFOB)
On day 7 and day 14, the cultured specimens were fixed in a 10 % formalin solution for 20 min, dehydrated in a series of alcohols, and processed with critical point drying technique for SEM examination. The SEM condition was the same as the paragraph previously mentioned.

As for the H&E sections, the cultured specimens were fixed in a 10 % formalin solution, embedded in paraffin, and sectioned at 4 μm. Section samples were stained with H&E for microscopic examination.

Guided tissue regeneration (GTR) in the canine model

One-wall intrabony defect animal model
The one-wall intrabony defect, split-mouth model was designed according to Lee's method.[35,36] Three medium-sized Mongrel dogs (7–13 kg) were chosen, and all lower 3rd premolar (P3) and lower 1st molar (M1) were first extracted. After ten weeks of healing interval, two 5 mm × 4 mm single-wall bone defects were created on each quadrant at the mesial and distal aspects of mandibular 4th premolars. Two reference notches had been made by high-speed carbide burs to record the upper and lower position of each side of the intrabony defect. Twelve defect sites from 3 dogs were randomly distributed into three groups (T, PC, NC) according to the different membranes placed as described (Table 1). The animal study protocol was approved by the Institutional Animal Care and Use Committee of National Taiwan University Hospital (Approval No. 20130260).

Anesthesia
General anesthesia of the animal was conducted by intramuscular injection of 2 ml Zoletil 50 (50 mg/ml, 7–25 ml/kg body weight) and Rompun 1 ml (2 %, 1 ml/10 kg body weight). An additional 0.5 ml atropine was added to

Table 1 Surgical site and group allocation in each animal.

Dog	Dog 1		Dog 2		Dog 3	
Defect side	R	L	R	L	R	L
Mesial	T	NC	PC	PC	PC	NC
Distal	T	PC	T	NC	NC	T

R = right side, L = left side.
T = Test group (BioOss® + dSIS membrane), PC = Positive control (BioOss® + BioGide®), NC = Negative control (BioOss® only).

decrease the saliva secretion. Before the surgical procedures, Xylestesin-A was applied at each site for local anesthesia and to decrease intraoperative bleeding.

Surgical procedures of guided tissue regeneration/bone grafting

The detailed surgical procedures of guided tissue regeneration/bone grafting (Fig. 2) are listed as follows.

1. An aseptic procedure was performed with 0.12 % chlorhexidine intra- and extra-orally. Draping was done.
2. Local anesthesia was done with Xylestesin-A.
3. A mid-crestal incision was made at the edentulous area mesial and distal to the bilateral 4th mandibular premolars with the 15c blade, along with an intrasulcular incision of the 4th premolars and one tooth mesial and distal to it. Then a mucoperiosteal flap was reflected.
4. A reference notch (N2) was placed on the mesial and distal root surfaces of the 4th premolars at the level of the bone crest before defect creation.
5. A total of twelve one-wall intrabony defects sized 4 × 5 mm (mesio-distal width and apico-coronal height) were created bilaterally on the mesial and distal sides of the 4th mandibular premolars.
6. The cementum was removed inside the defect area using Gracey curettes and chisels.
7. Another reference notch (N1) was placed on the mesial and distal root surfaces at the base of the defect.
8. Deproteinized bovine bone minerals, Geistlich Bio-Oss®, were mixed with blood collected during the surgery. The materials were placed into all one-wall intrabony defects.
9. The bone graft materials were then covered by the dSIS membrane (T group) or Geistlich BioGide® (PC group). The vertical level of the barrier membranes was aligned with the upper reference notch (N2). No membrane was placed over the defect in the NC group.
10. After releasing the incision, the periosteum was incised for flap advancement. 5-0 Nylon was used for the primary closure.
11. All animals received prophylactic antibiotic therapy with amoxicillin (10 mg/kg) and pain control with aspirin (10 mg/kg) twice daily for 3 days.
12. The sutures were removed 1 week after the surgery, and the healing condition was recorded.
13. Mouth cleaning and surgical sites irrigation with 0.12 % chlorhexidine were performed every week until the sacrifice of the animals.
14. Fluorescent dyes were injected subcutaneously to label the new bone formation at the site of the intrabony defect. Calcein green (20 mg/ml/kg BW, SIGMA-ALDRICH®, St. Louis. MO, USA) was injected on day 0, alizarin complexone (30 mg/ml/kg BW, Fluka®

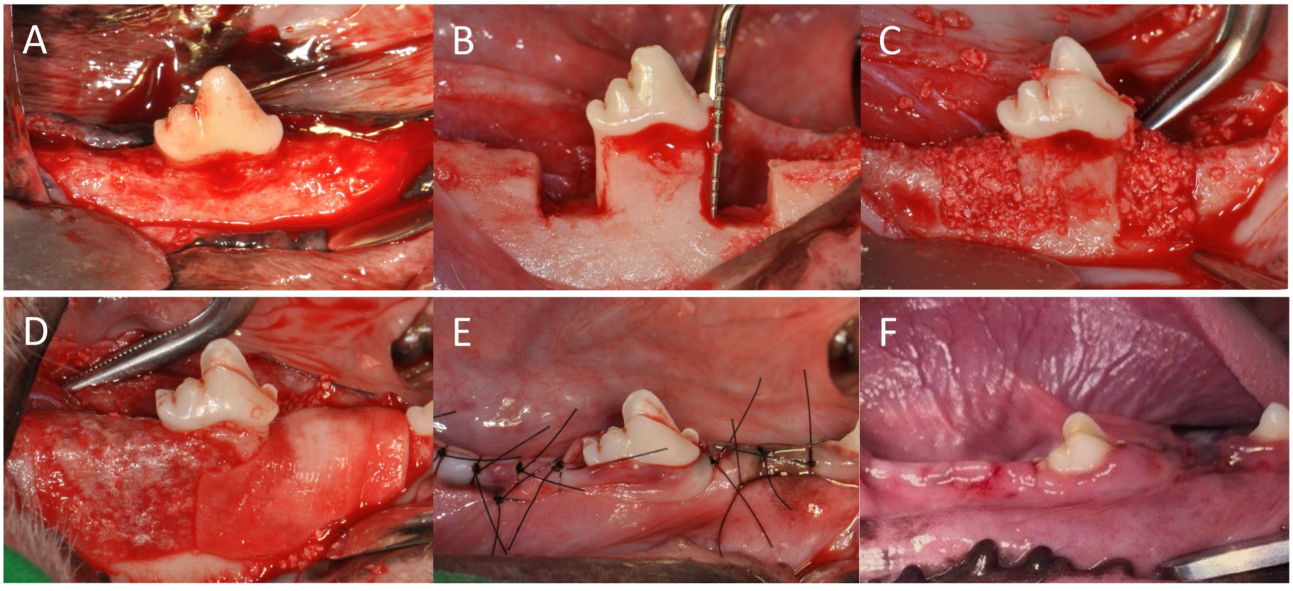

Figure 2 Procedures for the guided tissue regeneration. (A) Intact alveolar ridge before defect preparation. (B) Two 5 × 4 mm one-wall intrabony defects were created at the mesial and distal sides of each mandibular fourth premolar. (C) The BioOss was used to fill the experimental defects. (D) The assigned membrane covered each defect. (E) The sutures were placed with 5–0 nylon. (F) The sutures were removed one week after the surgery.

Analytical, Buchs, Switzerland) was injected on day 28, and tetracycline (25 mg/kg BW, Santa Cruz Biotechnology®, Dallas, TX, USA) was injected on day 56 after the surgery.

Histological fixation processing

All animals were sacrificed 12 weeks following the National Taiwan University Hospital guidelines for the euthanasia of animals. The defect site was first fixed by the perfusion-fixation method and dissected from the surrounding soft and hard tissue.[37] Additional fixation was performed by soaking the dissected tissue in 10 % buffered formalin for 1 week. Section samples were stained with H&E for microscopic examination.

Radiographic processing

All samples were first scanned by microcomputed tomography (Bruker SkyScan 1176 in vivo micro-CT, Kontich, Belgium) after formalin fixation. The images were acquired transverse to the tooth's longitudinal axis in a high-resolution mode at 18 μm, 80 keV, and 313 μA. The image data sets were then reconstructed in Dataviewer, and the region of interest (ROI) was defined.

Decalcified specimen preparation

The samples were split in half after CT data collection. One-half of the tissue blocks were first soaked in 20 times their volume of decalcifying solution EDTA for 72 h, then washed with the distilled water for 30 min. The above procedures were repeated several times until the decalcification was complete. After a thorough rinse with the distilled water, the specimens were dehydrated in an ethanol series (70 %, 80 %, 90 %, 95 %, 100 %) and embedded in paraffin-based embedding media. The specimens were trimmed to a thickness of 5 μm and stained with H&E.

Epoxy-resin embedded specimens for fluorochrome labeling observation

The other half of the samples were impregnated with the epoxy resin (Epothin, Buehler Ltd., Lake Bluff, IL, USA) in a vacuum impregnation system (Cast n' vac 1000, Buehler Ltd., Lake Bluff, IL, USA). After curing, the tissue blocks were trimmed, vacuumed, and mounted on the slides. The slides, mounted on the thin-sectioning system (PetroThin®, Buehler Ltd.), were further trimmed to 100—200 μm thickness for observation of fluorochrome labeling.

Radiographic analysis

The new bone volume (%) represented the percentage of newly formed bone in the defect. For each sample, the ROI in the micro-CT images was defined and rotated in Dataviewer (v.1.5.2.4, 64-bit, Bruker Co., Kontich, Belgium) to the correct orientation, so that one of the images corresponded to the decalcified histological slides.

For understanding the bone remodeling of the entirety in a one-wall defect, the ROI (Fig. 3) was set as 5 (height) × 4 (M-D width) mm^2 covering the entire one-walled bone defect. The buccal-lingual width (B-L width) was defined as a 2 mm extension from the center of the root to reduce the difference caused by the turning point of the dental arches.

Once the data had been recorded, the images were then transferred to the CTAn software (CT-Anlyser v.1.13, Bruker Co., Kontich, Belgium) to decide the grey thresholds at which the size and shape of the new bone on the micro-CT image would resemble one on the histologic slides. As a result, the lower and upper grey thresholds for the new bone area were defined as 47 and 80, respectively. Within these gray threshold values, most of the graft particles were excluded from the volume calculation, and most of the new bones were included in the volume calculation. After volume calculation, the new bone volume (nBv, %) of each sample was acquired.

Histologic/histometric analysis

The images of H&E-stained decalcified sections were digitalized by a digital pathological scan system (Aperio ScanScopes system, Aperio Technologies, Vista, CA, USA) and evaluated by a digital pathological analysis system (Aperio ImageScope, AperioTechnologies).

The images were observed under 10 × to scale 200 × , and the measured parameters for evaluating the efficacy of the regeneration were modified from CK Lee's study,[35] includes defect height (DH), junctional epithelium (JE), new cementum (nC), new bone height (nBh), and new bone area (nBa).

1. Defect height (DH): distance between upper notch (N2, level of the original bone crest) and lower notch (N1, level of defect base).
2. Junctional epithelium migration (JE): The distance between the apical extension of the junctional epithelium (aJE) and upper notch (N2).
3. New cementum (nC): The distance between the lower notch (N1) and the coronal extension of new cementum (cnC).
4. New bone height (nBh): The distance between the lower notch (N1) and the coronal extension of new bone (cnB).
5. New bone area (nBa): (Regenerated new bone area/total area of bone defect) × 100 %

Fluorochrome labeling observation

After trimming the epoxy-resin embedded specimens, we observed the slides at different excitation wavelengths corresponding to different chelating agents, calcein at 486 nm,[38] alizarin complexone at 605 nm, and tetracycline at 396 nm.[38] The images were first validated via fluorochrome labeling in the incremental line of dentin from the pulp cavity using a confocal laser scanning microscope (Carl Zeiss LSM 880, Jena, Germany) to determine the pattern and timeline of bone remodeling.

Statistical analysis

Statistical analysis was performed using statistical software (GraphPad Software, La Jolla, CA, USA). All data were

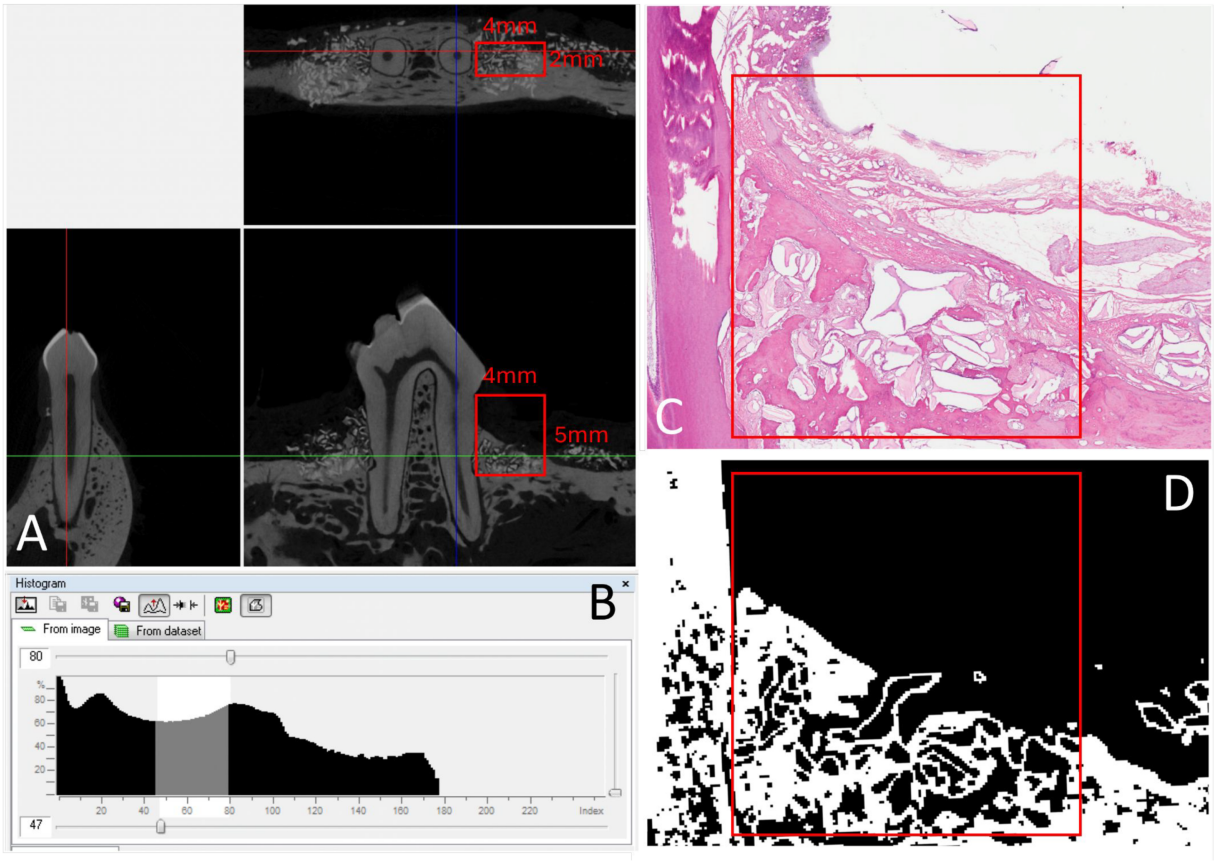

Figure 3 The calculation method of the percentage of new bone volume (%) (A). Refer to the decalcified tissue section, adjust the computer tomography file to the correct axial direction in the Data Viewer, and the red frame indicates the first region of interest (ROI): $5 \times 4 \times 2$ mm^3; (B, C and D) Export the file to CTAn. Adjust the grey threshold to 47–80. The image within the range is similar to the tissue section. Then, calculate the white area in the red frame. The white integral area represents the percentage of new bone volume in the bone defect (new bone volume, nBv, %). (For interpretation of the references to color in this figure legend, the reader is referred to the Web version of this article.)

represented as the mean ± standard deviation (Mean ± SD). A one-tailed unpaired Student's *t*-test was performed on the characterization data. A one-way analysis of variance and a Tukey post hoc test were used to assess multiple comparisons in the one-wall intrabony defect animal model. *P*-value <0.05 was considered statistically significant. *P*-value <0.001 was considered highly statistically significant.

Results

Characterization of scaffolds

The composition of the dSIS and BioGide®, including the content of amino acids, GAGs, and growth factors (VEGF-A and bFGF), was estimated (Tables 2 and 3). The total amino acid composition of the dSIS and BioGide® was determined. The hydroxyproline content of the dSIS and BioGide® was 13.825 ± 0.655 % and 13.125 ± 0.116 %, respectively. No statistical significance was found. The wt% of each amino acid was similar between the dSIS and BioGide®. The GAG content of the dSIS was 4.462 ± 0.212 μg/mg. The bFGF content of the dSIS was 120.988 ± 39.197 ng/g. The data indicate a significantly high amount of GAG and bFGF in the dSIS. No GAG or bFGF was detected in the BioGide®. No VEGF-A was detected in either group.

Scanning electron microscope (SEM) images for surface morphology

The ultrastructural morphology of the dSIS and BioGide® exhibited distinct architectural differences. The dSIS membrane exhibited a highly organized, interconnected network of collagen fibers (Fig. 5A). These fibers appeared relatively uniform in diameter, forming a fine, dense, but porous meshwork that maintained the structure of the natural extracellular matrix (ECM). In contrast, the cross-sectional view (Fig. 5B) reveals a distinctive, multilayered, lamellar structure, potentially providing superior tensile strength. On the other hand, the BioGide® (Fig. 5C and D) presented a more randomized and disordered fiber arrangement. The collagen bundles in the BioGide® appeared thicker and more "clustered" compared to the fine fibrillar structure of the dSIS.

Table 2 Amino acid composition of the dSIS and BioGide®.

AA	dSIS (Wt%)	BioGide® (Wt%)	*P*-value
D	5.950 ± 0.212	5.777 ± 0.038	NS
T	1.706 ± 0.112	1.998 ± 0.114	<0.001
S	3.613 ± 0.170	3.649 ± 0.024	NS
E	10.034 ± 0.362	10.386 ± 0.128	NS
G	24.348 ± 0.962	26.714 ± 0.221	<0.001
A	8.780 ± 0.358	11.391 ± 0.084	<0.001
C[a]	ND	ND	—
V	2.013 ± 0.007	3.456 ± 0.023	<0.001
M	0.769 ± 0.003	0.777 ± 0.005	<0.05
I	0.977 ± 0.127	1.138 ± 0.008	<0.05
L	3.156 ± 0.216	3.869 ± 0.026	<0.001
Y[a]	ND	ND	—
F	1.893 ± 0.161	2.484 ± 0.158	<0.001
K	1.522 ± 0.122	1.794 ± 0.012	<0.001
H	0.800 ± 0.003	0.539 ± 0.004	<0.001
R	7.685 ± 0.320	8.062 ± 0.155	NS
P	8.245 ± 0.476	8.525 ± 0.100	NS
W[a]	ND	ND	—
Hyp	13.825 ± 0.655	13.125 ± 0.116	NS

AA = amino acid, dSIS = decellularized small intestinal submucosa, ND = non-detectable, NS = non-significant.
[a] The amino acids C, Y, and W exhibit low recovery rates due to the chemical instability of cysteine, tyrosine, and tryptophan under standard acid hydrolysis conditions.

Table 3 Glycosaminoglycans and growth factors content of dSIS and BioGide®.

Item	dSIS (μg/mg)	BioGide® (μg/mg)	*P*-value
GAG	4.462 ± 0.212	0.000 ± 0.000	<0.001
bFGF	120.988 ± 39.197	0.000 ± 0.000	<0.001
VEGF-A	ND	ND	—

GAG = Glycosaminoglycans, bFGF = basic fibroblast growth factor, VEGF-A = Vascular endothelial growth factor A, dSIS = decellularized small intestinal submucosa, ND = non-detectable.

Osteoblast attachment and cell adaptation

As shown in the H&E section, seeded osteoblasts on the dSIS and BioGide® membranes were counted on days 7 and 14 (Fig. 4). After 7 days of culture (Fig. 4A and B), the hFOB 1.19 cells demonstrated excellent adaptation to the dSIS surface. However, this phenomenon was not observed in the cell-seeded BioGide®(Fig. 4C and D). Furthermore, the cell sheets on the dSIS and BioGide® were formed excellently on day 14 (Fig. 4E, F, G, and H), and no toxic effect on osteoblasts was observed. The H&E sections showed no apparent difference in cell morphology across any of the surfaces examined. The results also indicated that osteoblasts adhered and proliferated on the fibrous and rough surfaces.

As shown on the SEM, the hFOB 1.19 cells demonstrated excellent adaptation to the dSIS surface after 7 days of culture (Fig. 5E). The cells adopted a flattened, spindle-shaped morphology, with numerous filopodia extending to anchor onto the collagen fibers. By day 14 (Fig. 5F), both the dSIS and BioGide® surfaces were almost entirely occluded by a confluent layer of osteoblasts. Notably, different from the BioGide®(Fig. 5G and H), the cells on the dSIS appeared to integrate with the lamellar structure, suggesting that the intrinsic signaling molecules or the specific fiber topography of the dSIS may promote robust cell proliferation and the formation of a biological "bridge" across the membrane pores.

Table 4 The results of radiographic analysis of each group.

nBV(%)	NC	PC	T	*P*-value
ROI	24.70 ± 7.97	38.07 ± 16.15	37.34 ± 9.56	NS

nBv (%) = new bone volume in the defect/volume of the defect x100 %; NS = no statistical significance.

Guided tissue regeneration (GTR) in canine model

Clinical observation and gross examination

All wounds healed uneventfully after the surgery. There was no evidence of wound dehiscence, membrane exposure, loss of graft material, or infection during the healing period in all three animals. No discernible difference in wound healing was observed among the T group, PC group, and the negative control group.

Histologic analysis (decalcified specimen with H&E stain)

Twelve decalcified specimens were evaluated in this study. The black arrow on the graph (Fig. 6) represents the bottom of the notch N1 and N2. The red arrow indicates the highest point of the new bone on the root surface (new bone height, nBh). The blue arrows demonstrate the continuity of the highest new-bone position across the defect area.

The NC group (BioOss® only) (Fig. 6A): Apparent alveolar bone resorption and limited bone regeneration occurred. The soft tissue collapsed into the upper portion of the bone defect, and loss of bone grafting materials was also observed. A decreasing trend in the new bone height was observed with increasing distance from the root. Most decalcified Bio-Oss particles were deposited in the lower region of the defect. New bone formation was observed on the root surface and in the lower region of the defect, between the decalcified bone graft particles.

The PC group (BioGide® + BioOss®) (Fig. 6C): Compared with the NC group, less alveolar bone resorption was observed in the PC group. The bone defect area is mostly filled with new bone and decalcified Bio-Oss particles. The new bone height was highest near the root surface (red arrow). New bone formation was also observed far from the root surface. Although the new bone height decreases slowly (blue arrows), there were also many decalcified BioOss® particles and new bones between them. New bone formation was not only near the base of the defect and close to the root surface, but also at the upper portion of the defect and in areas distant from the root surface.

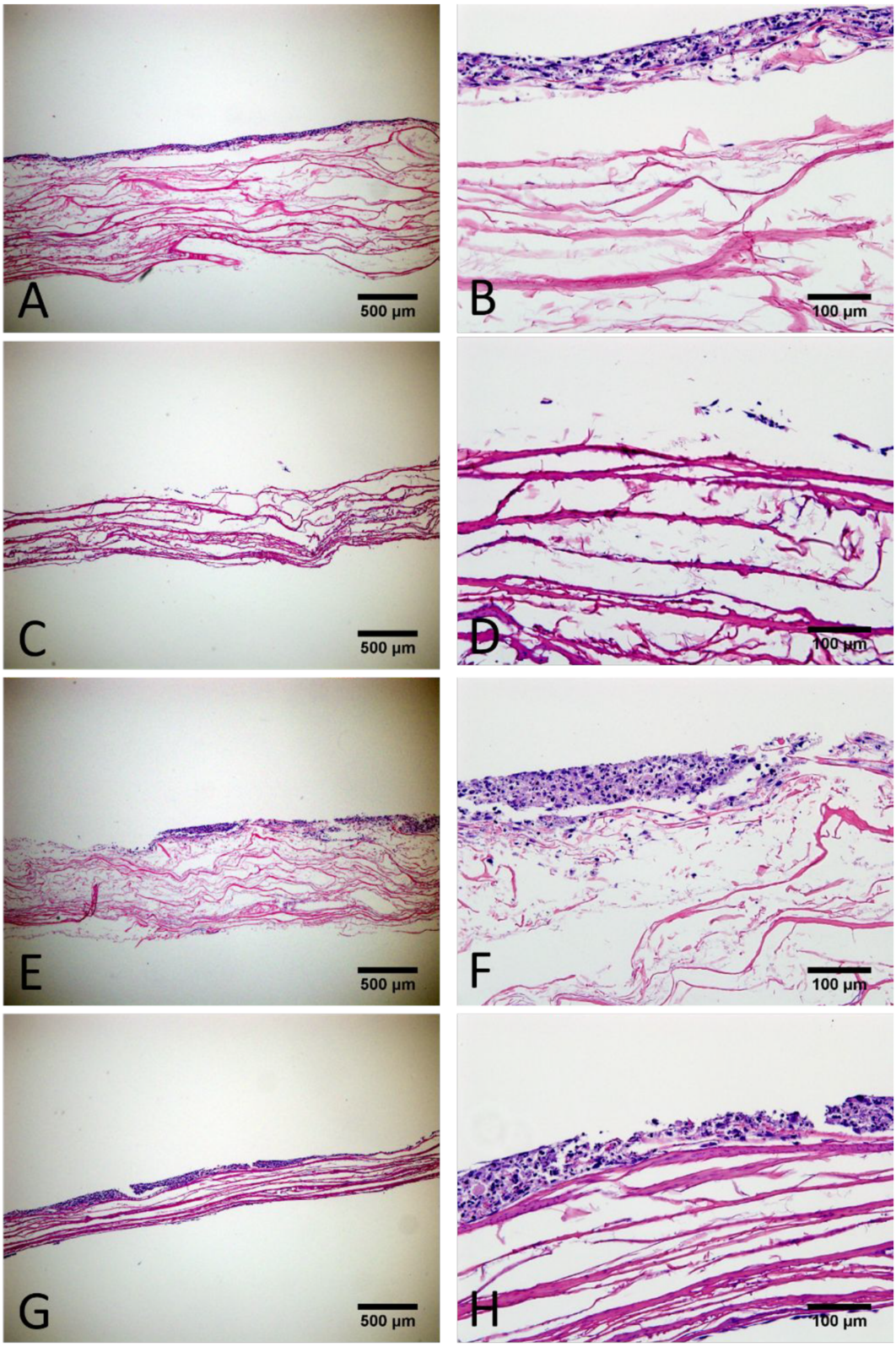

Figure 4 H&E sections of attachment of osteoblasts on the dSIS after 7 days (A and B) and 14 days (E and F), and on the BioGide® after 7 days (C and D) and 14 days (G and H).

The T group (dSIS + BioOss®) (Fig. 6E): Less alveolar bone resorption was observed in the T group compared with the NC group. More than half of the bone defect area was occupied by the new bone and decalcified Bio-Oss particles. The new bone height was highest near the root surface, and it appeared to be greater than that in the NC and PC

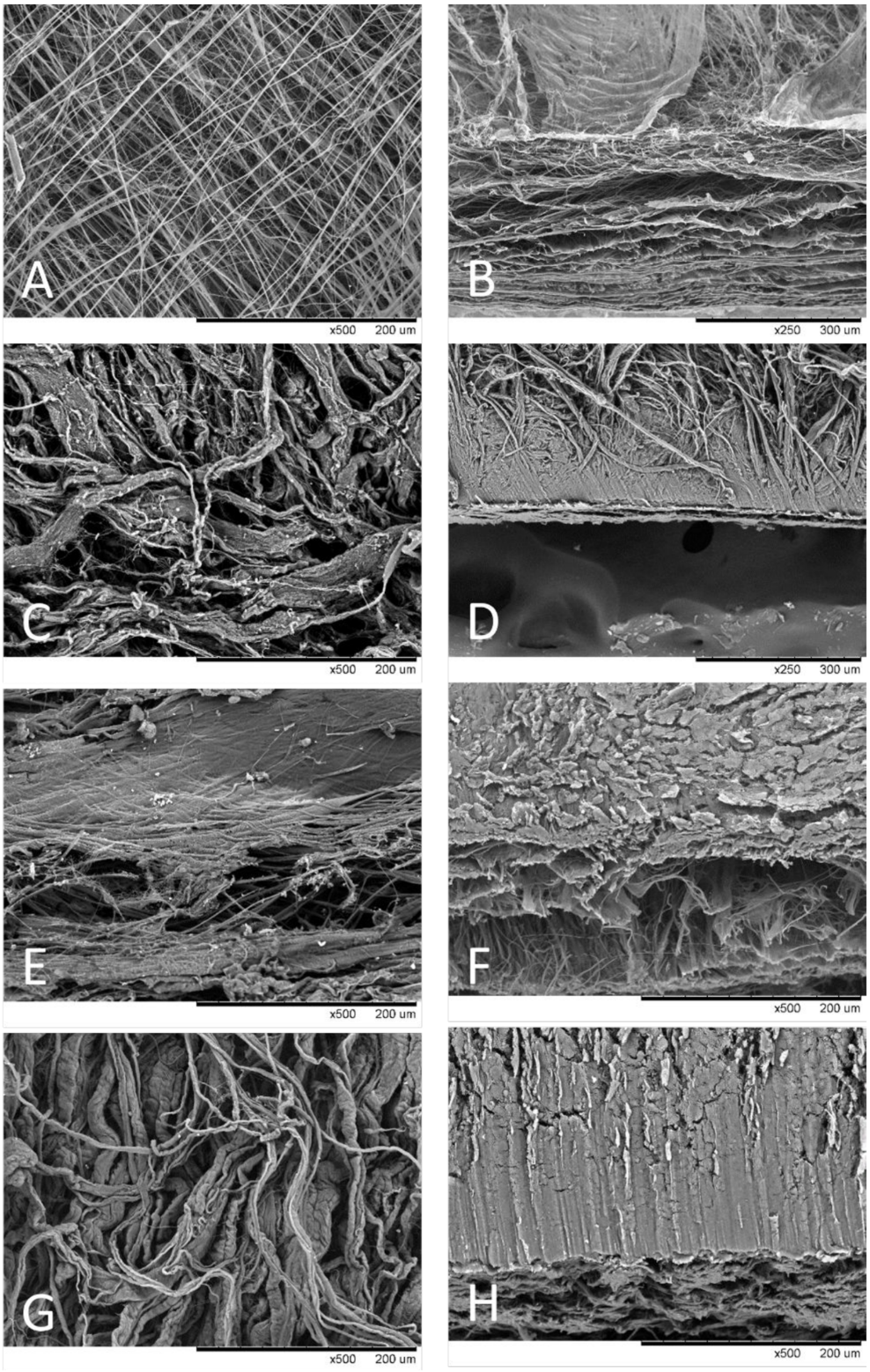

Figure 5 Scanning electron micrographs of the dSIS (A and B) and the BioGide® (C and D). Attachment of osteoblasts on the dSIS after 7 days (E) and 14 days (F), and on the BioGide® after 7 days (G) and 14 days (H).

groups. However, the new bone area decreased slightly with increasing distance from the root surface. The relative position of new bone formation was similar to that in the PC group. Furthermore, this section showed a larger, more intact new-bone area under the membrane than in the PC group.

In all groups, the junctional epithelium migrated and terminated at the N2 notch, with little difference. The new

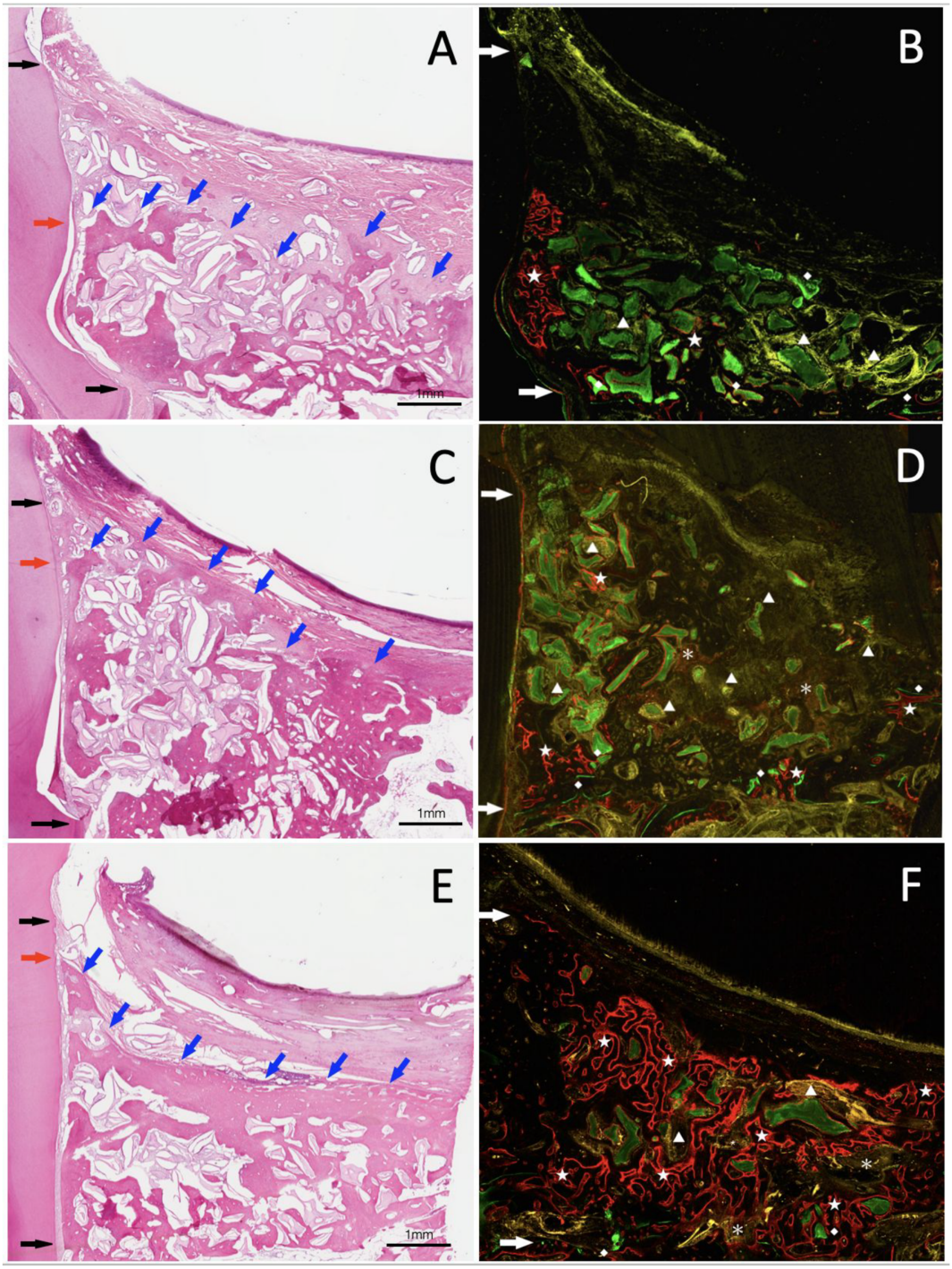

Figure 6 The comparison of the H&E section and fluorescence section. The left three graphs show the result of (A) NC, (C) PC, and (E) T group of H&E sections. The upper and lower black arrows represent the reference notch N2 and N1, respectively. The red arrow represents the new bone height on the root surface. The blue arrow represents the new bone height in the bone defect area. The right three graphs show the result of (B) NC, (D) PC, and (F) T group of fluorescence microscope observations. The left side of each graph implies the root position. The upper and lower white arrows represent the reference notch N2 and N1, respectively (◆: Calcein - green; ★: Alizarin complexone - red; ▲: Tetracycline - yellow; ✻: Bone remodeling area). (For interpretation of the references to color in this figure legend, the reader is referred to the Web version of this article.)

cementum extending from the coronal notch to the N1 notch was observed in all three groups, and the cementum became thinner as it grew coronally. No root resorption or ankylosis was observed in the study. The new collagen fibers forming in the periodontal ligaments of all groups extended perpendicularly or obliquely to the new bone and the new cementum.

Histometric analysis (decalcified specimen with H&E stain)

The average defect height (DH) in the NC, PC, and T groups was 5.23 ± 0.28 mm, 5.32 ± 0.52 mm, and 5.39 ± 0.56 mm, respectively ($P = 0.8913$). Those of the average junctional epithelium migration (JE) in the NC, PC, and T groups were 0.22 ± 0.24 mm, 0.99 ± 0.97 mm, and 0.57 ± 0.43 mm, respectively ($P = 0.2697$). Those of the average new cementum (nC) in the NC, PC, and T groups were 5.27 ± 0.47 mm, 5.39 ± 1.45 mm, and 5.49 ± 1.13 mm, respectively ($P = 0.9609$). Those of the average new bone height (nBh) in the NC, PC, and T groups were 3.29 ± 0.83 mm, 4.43 ± 1.29 mm, and 4.80 ± 0.98 mm, respectively ($P = 0.1635$). Those of the average new bone area (nBa) in the NC, PC, and T groups were 20.32 ± 8.59 %, 25.90 ± 12.22 %, and 23.77 ± 9.94 %, respectively ($P = 0.7506$).

All the parameters listed above were not statistically significant across these three groups. However, the data indicate a positive trend toward significance, especially for nBh in the T and PC groups compared with the NC group.

Radiographic analysis

Regarding the nBv% data for the ROI, the PC and T groups were higher than the NC group. The average of new bone volume (nBv) in the NC, PC, and T groups were 24.70 ± 7.97 %, 38.07 ± 16.15 %, and 37.34 ± 9.56 %, respectively ($P = 0.2486$) (Table 4).

Fluorochrome labeling observation

In general, green fluorescence accumulated around the BioOss® particle residues but not in the other area (Fig. 6). It is assumed that calcein green reagents chelate directly with calcium in the bone grafts because new bone remodeling had not yet occurred on day 0. Red fluorescence of alizarin complexone was observed on the surface of the root and at the outer margin of the bone defect. The yellow fluorescence of tetracycline was observed mostly at the defect center.

For the NC group (Fig. 6B), new bone formation began at the bottom of the defect at the root surface (0–4 weeks) and then extended to the area away from the root surface (4–8 weeks). Further bone remodeling was observed in the area away from the root surface (8–12 weeks).

In the PC group (Fig. 6D), new bone formation began at the bottom of the defect and at the side of the bone wall (0–4 weeks). It then migrated toward the center of the bone defect and toward the coronal position (4–8 weeks). Further bone remodeling was noted between 8 and 12 weeks.

In the T group (Fig. 6F), new bone formation began at the bottom of the defect and along the side of the bone wall (0–4 weeks). It then migrated toward the center of the defect, the root surface, and the area away from the root surface. The outer border of new bone formation was already determined at this time (4–8 weeks, shown in red). Further bone formation was noted toward the center of the defect, with no apparent bone growth toward the coronal portion, compared to the PC group.

Discussion

Regarding scaffold characterization, the decellularized matrix used in this study was primarily composed of proteins, so we employed amino acid analysis to profile the dSIS and BioGide® content. Some amino acids, such as proline and hydroxyproline, can be used to infer the collagen content in the decellularized matrix. Proline is incorporated into collagen in large amounts, and nearly half of it is hydroxylated. The amount of hydroxyproline in collagen is typically about 13–14 %. Therefore, quantitative hydroxyproline testing is a convenient method for measuring collagen content in the protein-based biomaterial scaffold. The hydroxyproline content of pure type I collagen is approximately 11.3 % by weight, as reported by Etherington and Sims.[39] In this study, the hydroxyproline content of dSIS and BioGide® was 13.825 ± 0.655 % and 13.125 ± 0.116 %, respectively. The higher weight percentage may be due to differences in the tissue type. No discernible difference between the two membranes could be found. These data indicate that both dSIS and BioGide® have a high collagen content.

Cell adhesion and migration are fundamental criteria for the membrane design. GAGs are essential components of the extracellular matrix, serving both structural and functional roles. The remaining GAG content might indicate the membrane's ability to modulate the healing process, including collagen fiber deposition, angiogenesis, and cell and tissue proliferation and differentiation.

In Mendoza-Novelo's study, 60 % of sulfated GAGs can be removed after decellularization with non-ionic detergents, and nearly 90 % can be removed by reversible alkaline swelling, reducing the GAG content from over 0.6 μg/mg to less than 0.1 μg/mg.[19] From Hodde's study, the total GAG content in the small intestinal submucosa is around 21 μg/mg.[40] In this study, no GAGs could be detected in the BioGide®. The GAG content in the dSIS was 4.462 ± 0.212 μg/mg. The APG/DHT/γ-radiation process removed almost 90 % of GAGs, but a relatively high amount remained in the membrane. The cell can easily bind to these components on its surface, thereby facilitating the cell adhesion and migration.

The basic fibroblast growth factor (bFGF) has been shown to promote cell proliferation and migration. Its interaction with GAGs has also been widely discussed. For example, heparin- or heparan sulfate-containing molecules are required for the high-affinity binding of bFGF to its receptor.[41,42] The amino acid homology between bFGF and VEGF-A has also been discussed. bFGF/VEGF-A is highly conserved among species,[43,44] and this conservation may contribute to the low lymphocyte attraction across species.[45] The similarity of the coding sequence may indicate possible utility in the human body. Our data showed similar results. bFGF from porcine can be detected by an anti-human bFGF antibody/horseradish peroxidase/streptavidin/3,3′,5,5′-tetramethylbenzidine system. The bFGF

content in the dSIS was 120.988 ± 39.197 ng/g. No bFGF was detected in BioGide®. In Jason's study, the bFGF content of the unprocessed SIS was 49.90 ± 1.02 ng/g. The amount of bFGF decreased to 26.74 ± 9.69 ng/g after peracetic acid/ethylene oxide sterilization.[46] Compared with our study, these data suggest that the APG/DHT/γ-radiation process may have greater potential for bFGF conservation.

As for VEGF-A, the data did not show the same pattern. VEGF-A concentrations could not be detected in dSIS or BioGide®. The diminished VEGF-A indicates that this growth factor, compared with bFGF, may be highly susceptible to this oxidative environment. In the overall evaluation of the dSIS and BioGide® composition, the data suggest that the BioGide® is a highly purified collagen membrane, and the dSIS contains the growth factors and GAGs that can enhance cell-binding ability.

The microstructure design is crucial for clinical use. Most dentists suggest that the GTR membrane design should be at least a 2-layer structure. The dense layer can prevent soft-tissue ingrowth into the augmented site, but the loose layer should degrade faster to support the cascade of biologic events leading to regeneration. Furthermore, decellularization methods have been reported to disrupt the microstructure of the ECM. To assess whether the membrane has a 2-layer structure and to evaluate structural damage on the dSIS and BioGide®, an SEM study was used to observe the microstructure of both membrane surfaces.

The SEM observation showed a gradient of porosity from top to bottom and from loose to dense in APG-treated dSIS. A multilayer gradient structure was suggestively visible at a 45-degree tilt. The distinctive gradient porous structure was controllable, and there was no obvious structural damage to the dSIS compared with the BioGide®.

Regarding the cell culture study, the images of the H&E section were consistent with the SEM images. The hFOB had infiltrated within 100 μm of the surface of both the dSIS and BioGide® on day 14. Both membranes showed no signs of cell infiltration or penetration. Both membranes, despite their different microstructures, demonstrated good cell–exclusion properties, which are necessary for a dental GTR membrane.

Furthermore, no hFOB sheets were found in the BioGide® group on day 7. The absence of an hFOB layer could result from (1) the layers not covering the entire membrane, so no cells appeared at the section margin. (2) hFOB on the BioGide® with limited adhesion properties could be washed out during the critical point drying process. Limited adhesion in the early stage may be due to the membrane composition. The dSIS, unlike BioGide®, preserves more biomolecules for cell adhesion, such as the GAGs and growth factors, which may promote the initial cell adhesion.

To delve deeper, regarding the histologic/histometric analysis in the canine model, in theory, the dSIS contains relatively high levels of GAG and growth factors. The retention of biomolecules, which may be highly immunogenic, could lead to more obvious inflammation. However, this was not observed in this study. The T group showed biocompatibility similar to that of the PC group, as assessed by microscopic and gross examination.

On microscopic examination, two additional phenomena could be observed in the histology section. One was the maturity of the new bone, and the other was the membrane's capacity to form spaces. The one-wall intrabony defect model used in this study was a good means of evaluating the membrane's space-making capacity, given its defect configuration. The space-making characteristic could be judged by the distribution of the highest position of the new bone. The PC group achieved the best results in space maintenance. The NC group was the worst, with the perceptible fibrous tissue around bone graft particles.

Regarding the maturity of new bone, most of the new bones were still woven and lamellar bones. Nearly all newly formed bones were occupied by the primary osteons and poorly organized across all the three groups after 12 weeks of implantation. Remodeled secondary osteons were hardly found. Compared with the PC group, the T group, with lower space-making capacity, had less fibrous tissue around bone graft particles and more mature, denser new bone at the interface of the dSIS membrane.

Overall, the histological evaluation of nBh and nBa in the T group and the PC control group was similar and relatively better than in the NC group. However, there was no statistically significant difference among these three groups.

Scholars have indicated the importance of the relationship between histometric and radiographic analyses.[47–49] The reliability of micro-CT data has also been validated by comparison with stereological histomorphometry. Park et al. further investigated and concluded that micro-CT analysis is not positively associated with histometric evaluation in the calculation of hard-tissue density.[50] The same results were observed in this study. Although these three groups showed no statistical significance in micro-CT analysis, as shown in the histometric analysis, there was still one difference: the nBv data indicate a more positive trend toward significance than the nBa data. The nBv data of the T and PC groups were similar, much better than those in the NC group, by more than 10 %. This is because the histology section, which is shown only in one plane, may not be representative of the entire specimen. Comparing the data from the 2-D histology with those from the 3-D scanning, the real bone remodeling results can be better interpreted.

The articles of intrabony defect animal models seldom discussed bone turnover rate and process. Therefore, fluorochrome labeling was used additionally for the evaluation of bone modeling process in this study. Accordingly, the theory of A-R-F sequence, which Frost[51] proposed, indicates that the basic multicellular units of bone remodeling occur throughout life in man and other large, long-lived animals. The remodeling process is about 6 weeks in rabbits and 12 weeks in canine. Assume that the signal of fluorochrome labeling would not lose during the remodeling process, the different chelating agents (calcein, alizarin complexone, and tetracycline) were injected for the evaluation of bone growth, regenerating, and remodeling in this study. The agents chelated the calcium ions and deposited them on the new bone area along with the progress of bone remodeling. On account of the similar fluorescence color of calcein and tetracycline, the time point of alizarin complexone injection was inserted between the two agents to avoid the overlap confusion of color response. The images were first validated via the fluorochrome labeling in the incremental line of dentin from the pulp cavity and were taken by the confocal laser scanning microscope (Carl Zeiss

LSM 880, Jena, Germany). The images were further blended to figure out the pattern and the timeline of bone remodeling.

Fluorochrome labeling study showed that the remodeling process of the T group was similar to the PC group. However, the PC group showed better bone height during the 8-week remodeling. Combined with the microstructure data, the PC group demonstrated a denser structure for better barrier function, so the osteoblasts under the membrane area could have a better chance for further remodeling in 8 weeks.

As for the earlier bone remodeling shown in the T group, the reason could be due to the composition difference between the T group and PC group. The reference mentioned that the matrix obtained by decellularization methods could contain GAG and the growth factor.[18,40] The trace amounts of these molecules could coordinate together to help the cell migration and adhesion.[41,52] In the composition analyses, the data showed that the membrane in the PC group was a pure collagen-based membrane. The membrane in the T group prepared by the decellularization method contained a small amount of GAGs and bFGF. Therefore, during dSIS degradation, the released biomolecules created a more favorable remodeling environment, supported signaling, and contributed to the host remodeling response in the early stage.

The APG-treated dSIS membrane contains a higher concentration of natural biomolecules (such as GAGs and bFGF) than the commercial product with the same indication. In addition to being more environmentally friendly, the APG/DHT/γ-radiation procedure may better retain adequate biomolecules. The in vitro data provide an outline of the dSIS-osteoblast interaction, which further supports this idea. Retained biomolecules may play an essential role in early-stage cell growth and adhesion.

Because the animal study was limited by the small sample size, statistical significance between groups could not be achieved in either histometric or micro-CT analyses. A trend was observed in which the test and positive control groups yielded better results than the negative control group. Accelerated bone healing, as assessed by the fluorescence bone labeling, was also observed in the dSIS group during the post-regeneration period. Establishing an experimental model that compares the histometric, micro-CT, and fluorescence bone labeling provides a novel approach for evaluating a new material for tissue regeneration.

In conclusion, although the evidence for a connection is not strong, the results suggest a possible correlation among the retention of biomolecules, osteoblast adhesion, and bone maturation. APG-treated dSIS membrane, compared with the traditional membrane, has similarly excellent biocompatibility and the potential to achieve good results in periodontal tissue regeneration from multiple perspectives.

Declaration of competing interest

The authors have no conflicts of interest relevant to this article.

Acknowledgments

Thanks to Yi-Hsuan Tsai for her assistance in editing the manuscript. The authors acknowledge the funding support from the project number NTUH 103-M2577 of National Taiwan University Hospital, as well as the project numbers NSTC113-2314-B002-059-MY3 and NSTC113-2314-B002-058-MY3 of the National Science and Technology Council, Taiwan.

References

1. Melcher AH. On the repair potential of periodontal tissues. *J Periodontol* 1976;47:256–60.
2. Scantlebury TV. 1982-1992: a decade of technology development for guided tissue regeneration. *J Periodontol* 1993;64(Suppl 11):1129–37.
3. Gottlow J. Guided tissue regeneration using bioresorbable and non-resorbable devices: initial healing and long-term results. *J Periodontol* 1993;64(Suppl 11):1157–65.
4. Hardwick R, Hayes BK, Flynn C. Devices for dentoalveolar regeneration: an up-to-date literature review. *J Periodontol* 1995;66:495–505.
5. Huang-Lee LL, Cheung DT, Nimni ME. Biochemical changes and cytotoxicity associated with the degradation of polymeric glutaraldehyde derived crosslinks. *J Biomed Mater Res* 1990;24:1185–201.
6. Ma B, Wang X, Wu C, Chang J. Crosslinking strategies for preparation of extracellular matrix-derived cardiovascular scaffolds. *Regen Biomater* 2014;1:81–9.
7. Bax DV, Davidenko N, Gullberg D, et al. Fundamental insight into the effect of carbodiimide crosslinking on cellular recognition of collagen-based scaffolds. *Acta Biomater* 2017;49:218–34.
8. Nyman S, Lindhe J, Karring T, Rylander H. New attachment following surgical treatment of human periodontal disease. *J Clin Periodontol* 1982;9:290–6.
9. Nyman S, Gottlow J, Karring T, Lindhe J. The regenerative potential of the periodontal ligament. An experimental study in the monkey. *J Clin Periodontol* 1982;9:257–65.
10. Haney JM, Nilveus RE, McMillan PJ, Wikesjo UM. Periodontal repair in dogs: expanded polytetrafluoroethylene barrier membranes support wound stabilization and enhance bone regeneration. *J Periodontol* 1993;64:883–90.
11. Cortellini P, Pini Prato G, Tonetti MS. Periodontal regeneration of human intrabony defects with titanium reinforced membranes. A controlled clinical trial. *J Periodontol* 1995;66:797–803.
12. Speer DP, Chvapil M, Eskelson CD, Ulreich J. Biological effects of residual glutaraldehyde in glutaraldehyde-tanned collagen biomaterials. *J Biomed Mater Res* 1980;14:753–64.
13. Farag A, Hashimi SM, Vaquette C, Bartold PM, Hutmacher DW, Ivanovski S. The effect of decellularized tissue engineered constructs on periodontal regeneration. *J Clin Periodontol* 2018;45:586–96.
14. Song L, Ye J, Zhai X, et al. A composite membrane of decellularized small intestinal submucosa and polycaprolactone for bladder tissue engineering. *ACS Appl Bio Mater* 2025;8:8708–20.
15. Liao J, Joyce EM, Sacks MS. Effects of decellularization on the mechanical and structural properties of the porcine aortic valve leaflet. *Biomaterials* 2008;29:1065–74.

16. Ott HC, Clippinger B, Conrad C, et al. Regeneration and orthotopic transplantation of a bioartificial lung. *Nat Med* 2010;16:927–33.
17. Goncalves AC, Griffiths LG, Anthony RV, Orton EC. Decellularization of bovine pericardium for tissue-engineering by targeted removal of xenoantigens. *J Heart Valve Dis* 2005;14:212–7.
18. Reing JE, Brown BN, Daly KA, et al. The effects of processing methods upon mechanical and biologic properties of porcine dermal extracellular matrix scaffolds. *Biomaterials* 2010;31:8626–33.
19. Mendoza-Novelo B, Avila EE, Cauich-Rodriguez JV, et al. Decellularization of pericardial tissue and its impact on tensile viscoelasticity and glycosaminoglycan content. *Acta Biomater* 2011;7:1241–8.
20. Lovekamp JJ, Simionescu DT, Mercuri JJ, et al. Stability and function of glycosaminoglycans in porcine bioprosthetic heart valves. *Biomaterials* 2006;27:1507–18.
21. Savic S, Lukic M, Jaksic I, et al. An alkyl polyglucoside-mixed emulsifier as stabilizer of emulsion systems: the influence of colloidal structure on emulsions skin hydration potential. *J Colloid Interface Sci* 2011;358:182–91.
22. Zhang F, Gu W, Xu P, et al. Effects of alkyl polyglycoside (APG) on composting of agricultural wastes. *Waste Manag* 2011;31:1333–8.
23. Messinger H, Aulmann W, Kleber M, Koehl W. Investigations on the effects of alkyl polyglucosides on development and fertility. *Food Chem Toxicol* 2007;45:1375–82.
24. Löffler H, Happle R. Profile of irritant patch testing with detergents: Sodium lauryl sulfate, sodium laureth sulfate and alkyl polyglucoside. *Contact Dermat* 2003;48:26–32.
25. von Rybinski W, Hill K. Alkyl polyglycosides—properties and applications of a new class of surfactants. *Angew Chem Int Ed Engl* 1998;37:1328–45.
26. Wess TJ, Orgel JP. Changes in collagen structure: drying, dehydrothermal treatment and relation to long term deterioration. *Thermochim Acta* 2000;365:119–28.
27. Schlegel AK, Mohler H, Busch F, Mehl A. Preclinical and clinical studies of a collagen membrane (Bio-Gide). *Biomaterials* 1997;18:535–8.
28. Geistlich ZE, Boyne P. Resorbable collagen membrane for use in guided tissue regeneration. *United States patent US5837278A* 1998.
29. Rothamel D, Schwarz F, Sager M, et al. Biodegradation of differently cross-linked collagen membranes: an experimental study in the rat. *Clin Oral Implants Res* 2005;16:369–78.
30. Schwarz F, Rothamel D, Herten M, et al. Angiogenesis pattern of native and cross-linked collagen membranes: an immunohistochemical study in the rat. *Clin Oral Implants Res* 2006;17:403–9.
31. Heinz Lussi PG. Process for preparing high purity bone mineral. *United States patent US5167961A* 1992.
32. Otter DE. Standardised methods for amino acid analysis of food. *Br J Nutr* 2012;108(Suppl 2):S230–7.
33. United States Pharmacopeia Convention. *Small intestinal submucosa wound Matrix—Glycosaminoglycan content test*. Rockville (MD): United States Pharmacopeia, 2007.
34. United States Pharmacopeia Convention. *Small intestinal submucosa wound Matrix—Fibroblast growth factor-2 content test*. Rockville (MD): United States Pharmacopeia, 2007.
35. Lee CK, Koo KT, Kim TI, et al. Biological effects of a porcine-derived collagen membrane on intrabony defects. *J Periodontal Implant Sci* 2010;40:232–8.
36. Lee CK, Koo KT, Park YJ, et al. Biomimetic surface modification using synthetic oligopeptides for enhanced guided bone regeneration in beagles. *J Periodontol* 2012;83:101–10.
37. Koenig H, Groat RA, Windle WF. A physiological approach to perfusion-flxation of tissues with formalin. *Stain Technol* 1945;20:13–22.
38. van Gaalen SM, Kruyt MC, Geuze RE, et al. Use of fluorochrome labels in in vivo bone tissue engineering research. *Tissue Eng Part B Rev* 2010;16:209–17.
39. Etherington DJ, Sims TJ. Detection and estimation of collagen. *J Sci Food Agric* 1981;32:539–46.
40. Hodde JP, Badylak SF, Brightman AO, Voytik-Harbin SL. Glycosaminoglycan content of small intestinal submucosa: a bioscaffold for tissue replacement. *Tissue Eng* 1996;2:209–17.
41. Yayon A, Klagsbrun M, Esko JD, et al. Cell surface, heparin-like molecules are required for binding of basic fibroblast growth factor to its high affinity receptor. *Cell* 1991;64:841–8.
42. Ornitz DM, Yayon A, Flanagan JG, et al. Heparin is required for cell-free binding of basic fibroblast growth factor to a soluble receptor and for mitogenesis in whole cells. *Mol Cell Biol* 1992;12:240–7.
43. Klagsbrun M. The fibroblast growth factor family: structural and biological properties. *Prog Growth Factor Res* 1989;1:207–35.
44. Holmes DI, Zachary I. The vascular endothelial growth factor (VEGF) family: angiogenic factors in health and disease. *Genome Biol* 2005;6:209.
45. Teixeira S, Fernandes H, Leusink A, et al. In vivo evaluation of highly macroporous ceramic scaffolds for bone tissue engineering. *J Biomed Mater Res A* 2010;93:567–75.
46. Hodde J, Janis A, Ernst D, et al. Effects of sterilization on an extracellular matrix scaffold: part I. Composition and matrix architecture. *J Mater Sci Mater Med* 2007;18:537–43.
47. Fajardo RJ, Ryan TM, Kappelman J. Assessing the accuracy of high-resolution X-ray computed tomography of primate trabecular bone by comparisons with histological sections. *Am J Phys Anthropol* 2002;118:1–10.
48. Chappard D, Retailleau-Gaborit N, Legrand E, et al. Comparison insight bone measurements by histomorphometry and microCT. *J Bone Miner Res* 2005;20:1177–84.
49. Muller R, Van Campenhout H, Van Damme B, et al. Morphometric analysis of human bone biopsies: a quantitative structural comparison of histological sections and micro-computed tomography. *Bone* 1998;23:59–66.
50. Park YS, Kim S, Oh SH, et al. Comparison of alveolar ridge preservation methods using three-dimensional micro-computed tomographic analysis and two-dimensional histometric evaluation. *Imaging Sci Dent* 2014;44:143–8.
51. Frost HM. The skeletal intermediary organization. *Metab Bone Dis Relat Res* 1983;4:281–90.
52. Naik MU, Vuppalanchi D, Naik UP. Essential role of junctional adhesion molecule-1 in basic fibroblast growth factor–induced endothelial cell migration. *Arterioscler Thromb Vasc Biol* 2003;23:2165–71.